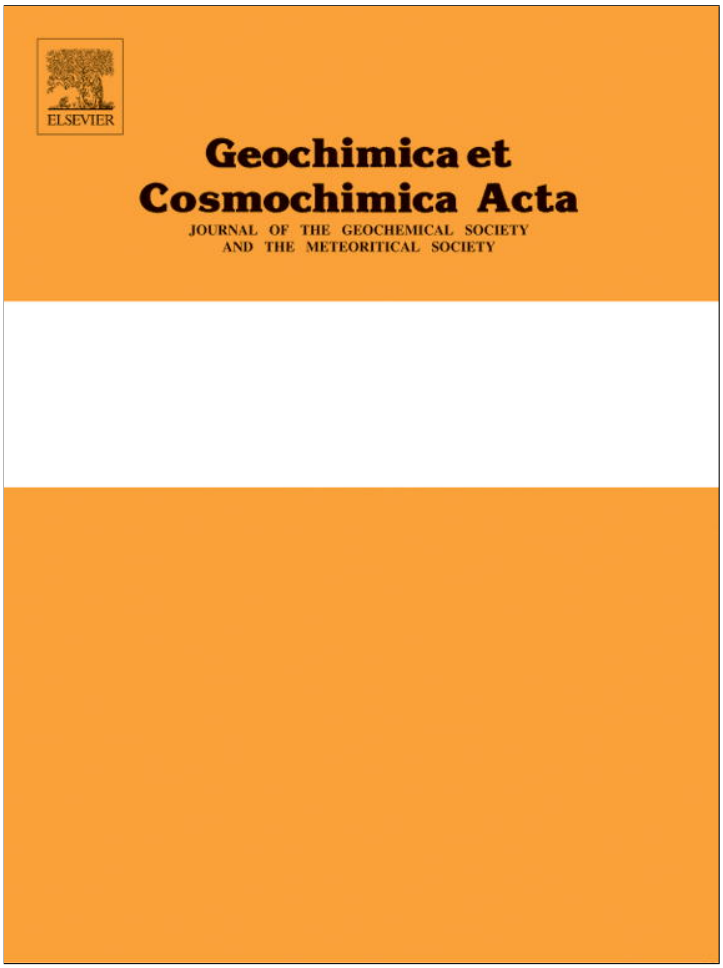

(This is a sample cover image for this issue. The actual cover is not yet available at this time.)

Available online at www.sciencedirect.com

SciVerse ScienceDirect

Geochimica et Cosmochimica Acta 104 (2013) 99–110

Geochimica et Cosmochimica Acta

www.elsevier.com/locate/gca

Precipitation, dissolution, and ion exchange processes coupled with a lattice Boltzmann advection diffusion solver

A. Hiorth [a,b,*], E. Jettestuen [a], L.M. Cathles [c], M.V. Madland [b]

[a] IRIS, P.O. Box 8046, N-4068 Stavanger, Norway
[b] University of Stavanger, N-4036 Stavanger, Norway
[c] Cornell University, Earth and Atmospheric Science, Ithaca, NY, USA

Received 31 August 2011; accepted in revised form 15 November 2012; Available online 29 November 2012

Abstract

Pore water chemistry can dramatically affect the mechanical strength of chalk cores and the recovery of oil from them, but despite a great many core experiments, the mechanisms responsible remain unclear. This is in part because no single model is presently available that can address the changes in surface complexes and potential and mineral dissolution and precipitation that occur when fluids of different chemistry are injected. We report here the construction of a lattice Boltzmann model that includes non-linear dissolution–precipitation kinetics, surface complexation, and ion exchange. A link-based boundary condition which allows mineral boundaries to move and porosity to change is shown to converge to a correct representation of the macroscopic pore surface area. We show the chemical LB model developed predicts mineral dissolution and ion exchange similar to those predicted by PHREEQC for similar parameters, and we show how the methods developed can be applied to chalk core experiments where synthetic seawater is flooded through the core at 130 °C.

1. INTRODUCTION

Flow-through chemical reaction experiments involving rock core are one of the most direct ways that laboratory experiments can be connected to the alteration that is produced by fluids moving through rocks or sediments in nature. Rock core experiments are, however, not always easy to interpret.

For example, very different explanations have been proposed for how injected waters might weaken chalk and affect oil recovery. Some have suggested that the dissolution of calcite due to secondary mineral formation might be responsible for the weakening (Madland et al., 2009, 2011), and that this dissolution might also undermine oil-wet portions of the chalk, liberate the oil, and increase oil recovery (Hiorth et al., 2010). But others suggest that these same effects are triggered by the changes in surface charge induced by sulphate injected and substitution of calcium adsorbed at the pore wall for magnesium (Zhang et al., 2007). Water composition impacts the rock mechanical strength of chalk cores, especially when magnesium rich brines are injected at temperatures around 130 °C (Madland et al., 2009, 2011). Furthermore, the mineralogy of the core affects weakening (Madland et al., 2009, 2011), and the exact location of minerals and the nature of their alteration seems to be important. In addition to all these processes, increasing the concentration of divalent ions in water injected into a chalk core can increase the production of oil by enhancing the spontaneous imbibition of water (Zhang et al., 2007). And in contrast to chalk, where the effect is usually the opposite, it has been found that lowering the salinity of injected water causes more oil to be produced from a sandstone core (Yildiz and Morrow, 1996; Tang and Morrow, 1999; Jerauld et al., 2006).

Many core flow-through chemical experiments have been performed over many years, but, as indicated in the previous paragraph, outcomes are diverse, affected by many variables, and the underlying causes of the phenomena

* Corresponding author at: IRIS, P.O. Box 8046, N-4068 Stavanger, Norway.
E-mail address: ah@iris.no (A. Hiorth).

0016-7037/$ - see front matter © 2012 Elsevier Ltd. All rights reserved.
http://dx.doi.org/10.1016/j.gca.2012.11.019

observed in many cases remain unclear. To make progress in this data-rich but complex context, methods are needed that can simulate how water injected into a rock core moves through the pore geometry of the core, contacts and interacts with individual mineral grains, forms complexes on the mineral surfaces, and changes surface charge. The purpose of this paper is to describe methods we have developed to do these things.

In the lattice Boltzmann (LB) model we develop we specify the chemistry of the injected fluid in terms of the total concentrations of a basis set of chemical species and advect and diffuse these total concentrations through the pores of the core using the LB flow field. After advection, a speciation calculation is performed at each node to determine the activity of individual species. Ion exchange is included, and the surface charge on all mineral surfaces is calculated. The pore fluid is then allowed to react with the mineral surfaces. The rate of dissolution and precipitation of an individual mineral is determined by a rate equation specific to each mineral phase.

The lattice Boltzmann methods (LBM) we employ are not new. LBM have been used to model reactive flow since 1992 (Kingdon and Schofield, 1992; Cali et al., 1992; Dawson et al., 1993; Chen et al., 1995). Dissolution of calcite has been studied using finite volume methods (Flukiger and Bernard, 2009). More recently Kang et al. (2010b) used the LBM to study how CO_2 injection into limestone forms dolomite and gypsum. Geochemical pore scale simulations have also been used to investigate the scale dependencies of geochemical reaction rates (Li et al., 2008; Molins et al., 2012) and to investigate calcite dissolution/precipitation in a microfluidic pore network (Yoon et al., 2012). Kang et al. (2010a) review the development of LB approaches for chemical reactions in both the pore space and at the fluid/solid interface.

We extend these previous models to include ion exchange and surface complexation. We also derive the LB boundary condition for nonlinear surface reaction kinetics that is similar to Kang et al. (2007), but implemented within the general surface orientation, placement and movement framework of Verhaeghe et al. (2006). We show that this new formulation converges to the actual surface area and provides a robust way to incorporate measured mineral dissolution and precipitation kinetics into LB models. The derived boundary condition corresponds to a backward Euler algorithm for the non-linear rate equation in the continuum limit.

The chemical model we use is based on the HKS equation of state and uses the SUPCRT geochemical database as implemented in EqAlt (Cathles, 2006). It can incorporate a very large number of minerals and complexes and can be used to 5 kbar pressures, temperatures up to 1000 °C (Johnson et al., 1992), and salinities up to about twice seawater. We show that our LB chemical simulations are nearly identical to PHREEQC (Parkhurst and Appelo, 1999). We illustrate the LB model developed by simulating the alteration produced when seawater is injected into chalk. We show how a single parallel plate LB pore geometry can simulate reactions in laboratory core experiments and we show that when this is done all the parameters (e.g. surface charge, surface complexes, and mineral dissolution and precipitation) needed to address water induced compaction and oil recovery are calculated. We do not pursue the application of these results to oil recovery and compaction in this paper, but will do so in subsequent publications. We do show that LB methods are able to match the effluent chemistry of core tests with little modification of independently-determined kinetic constants when seawater is injected into the core.

The LB algorithm for advection diffusion is briefly reviewed in the next section. In Section 2 we describe the combined LB-geochemical model. We assume the readers to be familiar with the basic LBM and geochemical calculations, which have been well described in the literature. However, we describe in detail the not-so-straight-forward, but critical, LB implementation of the chemical boundary condition. In Section 4 we compare the model with flow-through PHREEQC calculations and core experimental data. The last section provides a discussion and a summary and our conclusions.

2. THE LATTICE BOLTZMANN KINETIC, CHEMICAL-FLOW MODEL

Fluid flow and diffusion are simulated by standard LBM (Succi, 2001; Sukop and Thorne, 2006). At each grid point and for each of the discrete link directions, α, a distribution function of particles with the discrete velocity along α, is determined.

Collisions at the nodes redistribute the particle distribution functions in such a way that both mass and momentum are conserved. Boundary conditions for fluid flow are no slip, enforced by a mid-grid bounce back condition (Ziegler, 1993; He et al., 1997). A widely used version of the LBM is the BGK model (Chen and Doolen, 1998), where the collision operator is proportional to the distributions distance from equilibrium. We use the BGK-LB implementation in this paper.

The lattice Boltzmann velocity distribution at each grid point is described by f_α, where α indicates the velocity $\vec{e}_\alpha$ in the direction along the αth node link. The density of the fluid at a grid point is the sum of all the distributions at that grid point:

$$\rho(\vec{x},t) = \sum_\alpha f_\alpha, \tag{1}$$

and the mass flux of the fluid is:

$$\rho\vec{u}(\vec{x},t) = \sum_\alpha f_\alpha \vec{e}_\alpha. \tag{2}$$

The LB flow solution is formally equivalent to a solution of the incompressible Navier Stokes equation:

$$\frac{\partial\vec{u}}{\partial t} + (\vec{u}\cdot\nabla)\cdot\vec{u} = -\frac{1}{\rho}\nabla p + \nu\nabla^2\vec{u}. \tag{3}$$

We use the same method to solve for the advection and diffusion of the total concentrations of the chemical basis species in mol/L, $c_i(\vec{x},t)$:

$$c_i(\vec{x},t) = \sum_\alpha g_\alpha. \tag{4}$$

Here g_α is the velocity distribution function at each point of the total concentrations of the basis species i, where α again indicate the velocity direction on the grid lattice.

The advection velocity $\vec{u}$ is given by the LB fluid flow solution. This velocity is included in the advection–diffusion solution through the equilibrium distribution, $g_\alpha^{eq,i}$, used in the BGK-LB collision formulation, which depends on the flow velocity, Eq. (2), the total concentration of basis species, Eq. (4), and the link direction α:

$$g_\alpha^{eq,i} = \omega_\alpha c_i \left(1 + \frac{\vec{e}_\alpha \cdot \vec{u}}{C_2} + \frac{1}{2}\frac{(\vec{e}_\alpha \cdot \vec{u})^2}{C_2^2} - \frac{1}{2}\frac{\vec{u}^2}{C_2}\right), \tag{5}$$

where C_2 and ω_α are constants defined by the lattice. C_2 is a lattice parameter with the dimension of velocity squared. For the D2Q9 model used in this paper, $C_2 = 1/3$, and ω_α equals 1/9 for $\alpha = 1, 2, 3, 4$, equals 1/36 for $\alpha = 5, 6, 7, 8$ and $\omega_0 = 4/9$. The chemical lattice Boltzmann scheme is formally equivalent to a solution of the advection–diffusion equation (Wolf-Gladrow, 1995):

$$\frac{\partial c_i}{\partial t} + (\vec{u} \cdot \nabla c_i) = D\nabla^2 c_i. \tag{6}$$

The mathematics of the geochemical computation is cast in terms of basis species and secondary species (or complexes) (Johnson et al., 1992). The advective–dispersive lattice Boltzmann equations determine the total solution composition at the end of a time step. The $\log K$ of the dissociation reactions of the solution complexes determines the concentrations of the individual solution species and the total concentration of the basis species c_j in solution is:

$$c_j = m_j + \sum_{i=1}^{N_c} \mu_{ij} n_i, \tag{7}$$

where m_j is the concentration of basis species j, and n_i is the concentration of the complex i, N_c is the number of complexes, and μ_{ij} is the stoichiometric matrix of the complex dissociation reaction. Mass balance Eq. (7) can be inverted to give the log activity ratios of the basis species, and these ratios can be converted to basis species activities either by knowing the total concentration of H^+ or by obtaining it by requiring charge balance. In this paper we make sure that the influent solution and initial solution inside the system (core) is charge balanced by requiring that Eq. (7) is satisfied for all basis species, except H^+. We then require charge balance:

$$\sum_{i=1}^{N_b} Z_i m_i + \sum_{i=1}^{N_c} Z_i^c n_i = 0, \tag{8}$$

where Z_i and Z_i^c are the valence of the basis species and solution complexes. When Eqs. (7) and (8) is solved simultaneously, the activity of H^+ is determined. Once the total concentration of H^+ is known in the influent and initial solution there is no need for charge balance, and the total hydrogen concentration can be advected in the same fashion as the other basis species. This is a faster method than calculating charge balance after each advection–diffusion step, and we use this faster method in the calculations reported here. Where minerals are encountered on the pore walls we equilibrate the *initial* solution with these rock minerals using a basis switching technique (see e.g. (Bethke, 1996, chapter 4)).

The reactions at the walls require the dissolution $\log K$ of the wall minerals. We obtain the dissolution and dissociation $\log K$ from the HKF equation of state (Helgeson and Kirkham, 1974a,b; Helgeson et al., 1981) using thermodynamic data in the SUPCRT database (Johnson et al., 1992) and the program EQAlt (Cathles, 2006). A recent review of the HKF equation of state is given by Oelkers et al. (2009).

Ion exchange is included by adding one new basis species X with units of moles of cationic charge per liter of pore fluid as shown in Eq. (9). The effect is to capture exchange reactions as indicted in Eq. (10) (Appelo, 1994). The half reactions are a convenient means of achieving the physically meaningful exchange in (10). The $\log K$ values are taken to be small enough that the activity of X is negligible, alternatively one could exclude the concentration of X from Eq. (7). The advantage of this scheme is that ion exchange is accommodated within the solution chemistry description described above in a natural fashion.

$$\begin{aligned} &\mathrm{Na{-}X} \rightleftharpoons \mathrm{Na^+ + X^-}, \quad \log K = -20, \\ &\mathrm{Ca{-}X_2} \rightleftharpoons \mathrm{Ca^{2+} + 2X^-}, \quad \log K = -40.8, \\ &\mathrm{Mg{-}X_2} \rightleftharpoons \mathrm{Mg^{2+} + 2X^-}, \quad \log K = -40.6. \end{aligned} \tag{9}$$

$$\mathrm{2Na{-}X + Ca^{2+} \rightleftharpoons Ca{-}X_2 + 2Na^+}, \quad \log K = 0.8. \tag{10}$$

The activities of the exchange complexes are defined (Gaines and Thomas, 1953) as fractions of the cation exchange capacity (CEC) expressed in mol/L:

$$a_{i-X} = \frac{Z_i \gamma_i, m_{i-X}}{CEC}. \tag{11}$$

Note that the exchange complexes are electrically neutral. The ion exchange complexes are included in (7) by adding to the complexes n_i. The new basis species X is added to the basis species m_i in (7).

Surface complexes are added in the same fashion, following the approach of Van Cappelen et al. (1993). For similar models see Pokrovsky and Schott (1999, 2001, 2002), and Pokrovsky et al. (1999a,b). We define the disassociation of surface complexes (indicated by >) to surface basis species (>) and basis species. For example for calcite:

$$\begin{aligned} &\mathrm{>CaCO_3^-} \rightleftharpoons \mathrm{>CaH_2O^+ + HCO_3^- - H^+ - H^2O}, \\ &\mathrm{>CaOH^0} \rightleftharpoons \mathrm{>CaH_2O^+ - H^+}, \\ &\mathrm{>CaHCO_3^0} \rightleftharpoons \mathrm{>CaH_2O^+ + HCO_3^- - H_2O}, \\ &\mathrm{>CaSO_4^-} \rightleftharpoons \mathrm{>CaH_2O^+ + SO_4^{2-} - H_2O}, \\ &\mathrm{>CO_3H^0} \rightleftharpoons \mathrm{>CO_3^- + H^+}, \\ &\mathrm{>CO_3Ca^+} \rightleftharpoons \mathrm{>CO_3^- + Ca^{2+}}, \\ &\mathrm{>CO_3Mg^+} \rightleftharpoons \mathrm{>CO_3^- + Mg^{2+}}. \end{aligned} \tag{12}$$

All reactions are charge neutral. Each of these exchange reactions has a corresponding mass action equation from which an exchange $\log K$ can be defined. For example for the first line in Eq. (12):

$$>CaCO_3^- \rightleftharpoons >CaH_2O^+ + HCO_3^- - H^+ - H_2O,$$

$$K = \frac{a_{>CaH_2O^+}\, a_{HCO_3^-}\, \exp\{F\psi/(RT)\}}{a_{>CaCO_3^-}\, a_{H^+}\, \exp\{-F\psi/(RT)\}},$$

$$\log_{10}K = \log_{10}a_{>CaH_2O^+} + \log_{10}a_{HCO_3^-} - \log_{10}a_{H^+}, + 2\underbrace{\frac{F\psi}{\ln 10 RT}}_{\log_{10}E} - \log_{10}a_{>CaCO_3^-}. \quad (13)$$

Here we have assumed the activity of water is 1, Faradays constant $F = 9.648456 \times 10^4$ C/mol, and R is the ideal gas constant ($R = 8.314$ J/(K mol)), ψ is the surface potential and T is the absolute temperature. The activity of an aqueous species that is part of a surface complex is influenced by the surface potential, ψ, through the Boltzmann factor $\exp\{-Z_iF\psi/RT\}$, where Z_i is the valence of the basis species. If the surface potential has a negative sign then positively charged ions will have a high activity close to the surface and if the surface potential is positive, negatively charged ions will have a high activity close to the surface.

Compared to the usual disassociation $\log K$ equations, Eq. (13) has a new term that contains the surface potential ψ. We accommodate this addition by defining a new basis species with an activity E, such that $\log_{10}E \equiv F\psi/\ln 10RT$. This new basis species together with two new surface basis species, $>CaH_2O^+$ and $>CO_3^-$, are added to the basis species list m_j in (7).

The surface potential is related to the surface charge, σ, by the Grahame equation (see e.g. (Israelachivili, 1985)):

$$2\varepsilon\varepsilon_0 k_B T \sum_{i=1}^{N_b} m_i(\exp\{-Z_iF\psi/(RT)\} - 1) + 2\varepsilon\varepsilon_0 k_B T \sum_{i=1}^{N_c} n_i(\exp\{-Z_iF\psi/(RT)\} - 1) - \sigma^2 = 0, \quad (14)$$

where ε_0 is the dielectric constant of vacuum and ε is the dielectric constant of water, k_B is Boltzmanns constant, Z_i is the valence of the aqueous species ($Z_i = 0$ for the surface complexes), ψ is the surface potential, m_i is the concentration of a basis species, and n_i is the concentration of the aqueous or surface complex. The surface charge, σ in C/m^2, is proportional to the sum of all the charged surface complexes:

$$\sigma = \frac{F}{S}\left(\sum_{i=1}^{N_b} Z_{sci}\, m_i + \sum_{i=1}^{N_c} Z_{sci}\, n_i\right). \quad (15)$$

S is the surface area in m^2/L, the concentrations of the surface species, n_i, are in mol/L. Z_{sc} is the valence of a surface complexes. The surface complexes are included in n_i in (7) and their activities are calculated when the speciation calculation is done at a wall node.

Contrary to ion exchange complexes, the surface complexes in Eq. (12) are charged. In particular divalent ions from the solution can exchange with monovalent ions adsorbed at the surface. Thus when the solution advects past the pore surface, a charge imbalance in the pore fluid can build up, but we do not consider this in our calculations. We could extend our calculations to include the effect of the diffusive layer, by the method of Borkovec and Westall (1983) for example, but this would have only a minor effect on the predicted concentrations of the surface complexes (and hence surface charge and potential) and almost no effect on the aqueous solution concentrations at steady state. This is because the concentration of surface complexes is only dependent on the pore water composition, and in order for the diffusive layer to modify the pore water composition it has to have a thickness of the order of a fraction of the pore radius. At the high ionic strength we consider in this paper the thickness of the double layer is probably not larger than 1nm, which is much less than a typical pore size in chalk of the order of 1 μm.

Chemical reactions (dissolution, precipitation, surface complexation, ion exchange, etc.) at wall nodes are implemented in the boundary conditions. These boundary conditions relate the incoming (known) LB chemical distribution functions to the outgoing (unknown) LB distribution functions. The difference between the incoming chemical flux before and after colliding with a wall node is set equal to the chemical flux from the mineral dissolution or precipitation at that wall node as suggested by Bouzidi et al. (2001), Lallemand and Luo (2003), and Verhaeghe et al. (2006):

$$g_{\bar{\alpha}}^i - \tilde{g}_\alpha^i = (\omega_\alpha + \omega_{\bar{\alpha}})\frac{\vec{e}_{\bar{\alpha}} \cdot \mathbf{n} J_R^i}{C_2}, \quad (16)$$

where $\mathbf{n}J_R^i$ is the chemical flux for species i from chemical reactions at a mineral surface, $\mathbf{n}$ is the surface normal vector pointing towards the fluid phase, $g_{\bar{\alpha}}$ is the chemical flux reflected from the surface, $\tilde{g}_\alpha$ is the chemical flux into the surface, the lattice weights are chosen equal for velocities with same magnitude, i.e. $\omega_\alpha = \omega_{\bar{\alpha}}$, $\vec{e}_{\bar{\alpha}}$ is the direction of the chemical flux along the α link pointing away from the wall (i.e. $\vec{e}_{\bar{\alpha}} \cdot \mathbf{n}$ is always positive), and $C_2 = 1/3$ for the D2Q9 lattice.

For each link there are two unknowns, $g_{\bar{\alpha}}^i$, and c_i. Thus we need one more equation to close the system. For this purpose Eq. (5) is used along a link (ignoring terms of the order u^2, and by definition $\vec{e}_{\bar{\alpha}} = -\vec{e}_\alpha$):

$$g_{\bar{\alpha}}^i + \tilde{g}_\alpha^i = (\omega_\alpha + \omega_{\bar{\alpha}})c_i, \quad (17)$$

by combining this equation with Eq. (16), we find:

$$c_i = \frac{\tilde{g}_\alpha^i}{\omega_\alpha} + \frac{1}{C_2}(\vec{e}_{\bar{\alpha}} \cdot \mathbf{n})J_R^i. \quad (18)$$

Since J_R^i depends on the individual basis species concentrations m_i, we replace c_i using Eq. (7):

$$\frac{\tilde{g}_\alpha^i}{\omega_\alpha} = m_i + \sum_{j=1}^{N_c} \mu_{ji}\, n_j - \frac{1}{C_2}(\vec{e}_{\bar{\alpha}} \cdot \mathbf{n})J_R^i. \quad (19)$$

This equation applies to any area element of the pore wall that is intersected by a lattice link. The method of solution is to sum this equation for all wall-link intersections over a representative volume element while simultaneously determining the pore volume in that representative element. The appendix shows that the surface area seen by this LB boundary condition converges to the macroscopic surface area as the discretization increases. The LB boundary condition in Eq. (18) is equivalent in the continuum limit to the backward Euler algorithm (see e.g. Steefel and MacQuarrie (1996) p. 92).

J_R^i is specified by the chemical composition at the surface and a kinetic rate expression. A suitable rate equation is one suggested by Morse and Berner (1972), Steefel and Van Cappelen (1990), and Lasaga (1998):

$$\frac{dM_i}{dt} = \frac{A}{V} J_{\mathrm{M}}^i = \frac{A}{V} \mathrm{sgn}(1-\Omega_i)\left(k_1^i + k_2^i a_H\right)\left|1-\Omega_i^m\right|^n, \qquad (20)$$

where M_i is the concentration of mineral i (mol/L), A_i is the surface area of mineral i (m^2), V is the volume of fluid (L), Ω_i is the saturation index for mineral i, $k_{1,2}$ are rate constants (mol/m^2/s), m, and n are exponents indicating the order of reaction. The change in the total basis species concentration due to dissolution and precipitation can then be written:

$$\frac{dc_i}{dt} = \frac{A}{V} J_R^i$$
$$J_R^i = \sum_j v_{ij} \mathrm{sgn}(1-\Omega_j)(k_1 + k_2 a_H)\left|1-\Omega_j^m\right|^n, \qquad (21)$$

where the sum goes over all the minerals present at one node, v is the stoichiometric matrix, and A is the surface area of one wall node.

The boundary condition in Eq. (19) is solved once for each link that intersects a wall node in the following way:

1. Put the activity of all complexes to zero, and the activity of the basis species equal to the total basis species concentration.
2. Calculate the ionic strength.
3. Calculate the activity coeffecient of the species from the extended Debye-Huckel equation and thus the concentration of the species.
4. Solve Eq. (19) for the basis species activities by the Newton–Raphson method (if surface complexes are present, Eqs. (14) and (15) are solved for the surface potential and charge simultaneously with Eq. (19)).
5. Return to 2, until the pH and ionic strength change less than a specified tolerance.
6. Store amount of basis species adsorbed due to ion exchange or interaction with surface complexes. Determine the total basis species concentration, c_i, from Eq. (7) and calculate the outgoing LB distribution function, g_α^i, from Eq. (17).

3. COMPARISON OUR LB CHEMICAL MODEL TO PHREEQC

The chemical solver can be checked by comparing with PHREEQC (Parkhurst and Appelo, 1999). As there is no pressure dependent database in PHREEQC we compare our chemical solver with PHREEQC at 50 °C and 1 atm. The simulation example is simply a beaker with the initial solution given in the first column in Table 1. Dolomite and calcite are then added to the beaker and the solution equilibrate with the minerals present. The system is closed to the atmosphere (i.e. no equilibrium with CO_2(g)). The other columns in Table 1 list the final equilibrium concentrations. The range in the calculated concentrations, reflects the different databases used to define the disassociation and dissolution log$K$ values. Our calculation (the column to the right) lies between the PHREEQC values. Table 2 shows some of the major species predicted by the different calculations.

In Fig. 1 we have simulated ion exchange in a core where a calcite (chalk) core with a CEC of 0.25 mol/L initially in equilibrium with distilled water is flushed with a 0.219 M $MgCl_2$ solution at a flooding rate of 1 PV/day. We only consider ion exchange no chemical dissolution or precipitation. The simulation set up for the LB code is the same as discussed in the next section. As seen from Fig. 1, the LB predictions compares well with PHREEQC.

4. APPLICATION TO CORE EXPERIMENTS

The coupled LB-chemical kinetic model just described is illustrated by application to core flooding experimental data. We adopt the simplest possible LB model of flow between two parallel plates. The experimental data which we simulate are from an experiment in which Liege chalk outcrop cores were filled with distilled water and then flooded with synthetic seawater with low NaCl concentration at 130 °C (Madland et al., 2011). Core and LB parameters are given in Table 3.

The first step in modeling is to determine the lattice Boltzmann time step by requiring that the Péclet number in the simulations is equal to the Péclet number in the experiments. The Péclet number for the experiment is:

$$Pe = \frac{Lu}{D} = \frac{7\cdot 10^{-2}\ \mathrm{m}\ 1.05\cdot 10^{-6}\ \mathrm{m/s}}{7\cdot 10^{-9}\ \mathrm{m^2/s}} = 10.5, \qquad (22)$$

where L is the length of the core (7 cm), u is the Darcy flow velocity (1.3 pore volumes per day or 9 cm/day), and D is the aqueous diffusion constant at 130 °C ($= 7\times10^{-9}$ m^2/s corresponding to $D = 10^{-9}$ m^2/s at 25 °C, and an activation energy of 19 kJ/mol).

In the LB simulations the Péclet number is:

$$Pe = \frac{N_x u_{LB}}{\frac{1}{3}\left(\tau - \frac{1}{2}\right)}. \qquad (23)$$

In the simulations we use $\tau = 1$, $N_x = 40$, and $N_y = 8$. The average (Darcy) velocity in the pore model is then $u_{LB} = 0.044$. Fig. 2 shows the LB velocity profile in the tube, and compare with the analytical solution. LB particles advance one node each computational iteration, so the time increment corresponding to a LB iteration is 1.2 min:

$$\delta_t = \frac{u_{LB}}{u}\delta_x = \frac{Pe}{6N_x u}\frac{L}{N_x} = \frac{1}{6D}\left(\frac{L}{N_x}\right)^2$$
$$\delta_t = \frac{1}{6\cdot 7\cdot 10^{-9}\mathrm{m^2/s}}\left(\frac{7\cdot 10^{-2}\mathrm{m}}{40}\right)^2 = 1.2\ \mathrm{min}. \qquad (24)$$

The second and last step in the modeling is to determine the kinetic rate constants to be used in the simulation. Table 4 gives the values for the rate constants. For the parallel plate LB simulation:

$$\frac{A_{LB}}{V_{LB}} = \frac{2N_x\delta_x}{N_x N_y \delta_x^2} = \frac{2}{N_y\delta_x}. \qquad (25)$$

For the core experiment, however, the surface to volume ratio is A/V. Thus we want to scale the rate equation by:

Table 1
Comparison of the chemical solver with PHREEQC, the concentrations are in mol/L. Initial phases are dolomite and calcite, and the initial solution composition is $c_{Ca} = 10^{-8}, c_{Mg} = 0.219$, $c_{HCO_3} = 10^{-8}$, and $c_{Cl} = 0.438$ mol/L, five different databases has been run in PHREEQC.

Solution species	PHREEQC (minteq)	PHREEQC (llnl)	PHREEQC (phreeqc)	PHREEQC (pitzer)	PHREEQC (wateq4f)	LB solver
Ca	2.10E−01	1.26E−01	1.53E−01	1.63E−01	1.53E−01	2.09E−01
Mg	8.98E−03	9.35E−02	6.62E−02	5.61E−02	6.62E−02	1.02E−02
HCO_3	1.92E−05	5.09E−05	5.10E−05	3.13E−05	4.99E−05	3.14E−05
Cl	4.38E−01	4.38E−01	4.38E−01	4.38E−01	4.38E−01	4.38E−01
pH	8.12	7.79	7.74	7.82	7.74	7.83

Table 2
Some of the major complexes in the calculation, the concentrations are in mol/L.

Solution complex	PHREEQC (llnl)	PHREEQC (minteq)	PHREEQC (phreeqc)	PHREEQC (pitzer)	PHREEQC (wateq4f)	LB solver
CaCl	4.70E−03	–	–	–	–	4.52E−03
MgCl	8.41E−04	–	–	–	–	8.51E−04
$CaCl_2$	8.12E−04	–	–	–	–	6.17E−04
CaOH	1.31E−06	5.29E−06	4.41E−07	–	4.38E−07	1.04E−05
$CaHCO_3$	4.43E−06	1.54E−05	1.40E−05	–	1.27E−05	8.54E−06
OH	1.03E−05	5.74E−06	4.75E−06	1.78E−07	3.83E−06	7.82E−06

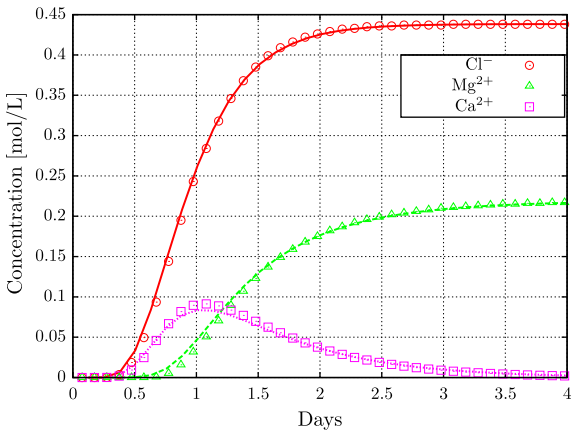

Fig. 1. Comparison with PHREEQC, solid lines are the LB results and the points PHREEQC simulation, CEC is set to 0.25 mol/L.

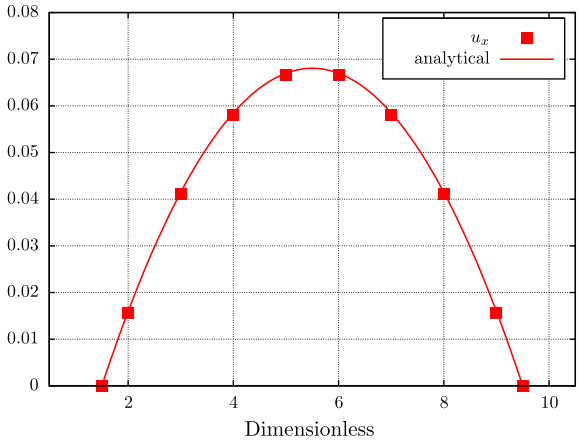

Fig. 2. Velocity profile in the tube. The solid line is the analytical solution for Poiseuille flow and the data points are the LB simulation of the velocity profile. Note that the maximum speed of 0.066 gives the average speed of 0.044 that is used in the simulations.

Table 3
Physical parameters describing the rock core used and the LB model. The parameters D, L, and u, are defined in the tex. The number of surface sites is taken from (Davis and Kent, 1990).

Physical parameters	Value	Simulation parameters	Value
D	7×10^{-9} m^2/s	τ	1
L	7 cm	N_x	40
u	1.1×10^{-6} m/s	N_y	8
Mass	100 g	γ	1.4×10^{-3}
Surface area	2 m^2/g		
Pore volume	30 ml		
Porosity	50%		
$>CaH_2O$ and $>CO_3$	2 sites/(nm)^2		

Table 4
Values of the rate constants at 130 °C used in the LB modeling.

Mineral	k_1 mol/m^2 s	k_2 mol/m^2 s	m	n	E_a kJ/mol	Ref.
Calcite	3.88×10^{-6}	0.125	1	1	37.8(k_1) 8.4(k_2)	Plummer et al. (1978)
Magnesite	2.74×10^{-11}	0	1	2	60	Saldi et al. (2009)
Anhydrite	2×10^{-10}	0	1	1	–	Fit to data

$$\frac{V_{LB}A}{A_{LB}V} = \frac{N_y}{2}\frac{\delta_x A}{V}, \tag{26}$$

and Eq. (18) become:

$$c_i = \frac{\tilde{g}^i_\alpha}{\omega_\alpha} + \frac{1}{C_2}(\vec{e}_{\overline{\alpha}} \cdot \mathbf{n})\frac{N_y}{2}\frac{\delta_x A}{V}J^i_{\mathrm{R}} = \frac{\tilde{g}^i_\alpha}{\omega_\alpha} + \frac{1}{C_2}(\vec{e}_{\overline{\alpha}} \cdot \mathbf{n})\frac{N_y}{2}\frac{\delta_t A}{V}J^i_{\mathrm{R}}. \tag{27}$$

J^i_{R} is given by Eq. (21).

The difference $g^i_{\overline{\alpha}} - \tilde{g}^i_\alpha$ is the change in moles per liter of specie i along the link α and the change in mols per liter pore fluid of the mineral j is then given by:

$$\frac{2}{N_y}\sum_i \nu^{-1}_{ji}(g^i_{\overline{\alpha}} - \tilde{g}^i_\alpha). \tag{28}$$

Note that the equation above assumes that the stoichiometric matrix ν has an inverse (i.e. the minerals are linearly independent). If the minerals contacted are not linearly independent, the mineral change is calculated from the mineral flux, J_{M}, given in Eq. (20).

Boundary conditions are needed at the inlet and outlet. At the outlet we impose the zero diffusive flux boundary condition $\nabla \cdot c_i = 0$. This is achieved by copying the distributions of the neighboring nodes in the upstream direction. The concentrations are specified for the injected fluid, but the high concentration gradients at the inlet need to be neutralized so that there is no loss or gain of mass due to the diffusion at the inlet. The following boundary condition achieves this purpose (see the appendix for derivation):

$$g^i_{\overline{\alpha}} - \tilde{g}^i_\alpha = (\omega_\alpha + \omega_{\overline{\alpha}})\frac{\vec{e}_{\overline{\alpha}} \cdot \vec{u}\, c^{\mathrm{inlet}}_i}{C_2}, \tag{29}$$

where $\vec{u}$ is the fluid velocity and c^{inlet}_i is the original concentration of chemical specie i in the injected fluid.

4.1. Results

Fig. 3a compare the LB simulations of the core effluent chemical data using the values in Table 4. The match between the LB predictions and the laboratory measurements is generally very good. The initial peak is matched largely because we have included ion exchange with the surface. After this peak, however, there is a small upward trend in the Mg concentration and a small downward trend in Ca concentration that is not matched by the simulation. The rate constant for anhydrite precipitation that gives the best fit to the observed effluent concentration history (2×10^{-10} mol/m^2/s) is very close to the value 9.6×10^{-10} mol/m^2/s (at 123 °C) found by Wagner et al., 2005, which they estimate from a core flooding experiment with a similar set up to ours. However, both our value and the one by Wagner et al. (2005) are much lower than the rate constant reported in Palandri and Kharaka (2004) of 6.5×10^{-4} mol/m^2/s (at 25 °C). The mineralogical alteration is shown in Fig. 3b. Magnesite and anhydrite precipitate, and calcite is dissolved.

In Fig. 4, the simulated surface potential and surface charge are shown along the core. Fig. 5 shows the corresponding concentration of the individual surface complexes along the LB core. As calcium, magnesium and sulfate in the seawater enter the core, they adsorb onto the chalk surface and the net effect is that the surface charge increases. The surface potential is related to charge by the Grahame Eq. (14), and for low surface potentials $\psi \sim \sigma/\sqrt{I_o}$. Since the core initially is filled with distilled water, the ionic strength initially is low and thus the surface potential is high in certain parts of the core even where the surface charge has not increased very much. For example near the discharge end of the core at the early stages of flooding the surface potential has increased much more than might be expected by the small increase in surface charge because I_o is still low. At steady state there is a gradient in the predicted surface charge and potential along the core. This is because of calcite dissolution, which creates a gradient in calcium concentration towards the discharge end. Thus more calcium is adsorbed (higher surface charge) near the discharge end than close to the inlet.

5. DISCUSSION AND CONCLUSIONS

We show in this paper how a LB model can be integrated with a LB geochemical model in a way that allows the calculation of local mineral dissolution and precipitation, local change in solution chemistry, local surface charge and potential, and local change in surface complexes. Our model includes nonlinear surface reaction kinetics similar to Kang et al. (2007), but applied within the framework of general surface orientation, and placement (Verhaeghe et al., 2006). Our LB chemical model agrees well with PHREEQC. We show in the appendix that the LB boundary conditions converge to the true surface area as the grid is refined.

The model is approximate in several regards. First we advect the total basis species concentrations rather than the individual species concentrations. Charge balance constraints will reduce the error associated with this approximation and the error is probably not significant. That this approximation has been made should be kept in mind. Second, we have adjusted the anhydrite precipitation kinetics to fit the experiments. Third, the surface complexation reactions induce a charge imbalance in the pore fluid.

We illustrate the LB model developed by simulating the chemical consequences of injecting artificial seawater into a chalk core. We show that the LB model does a good job in simulating the chemical changes observed with literature

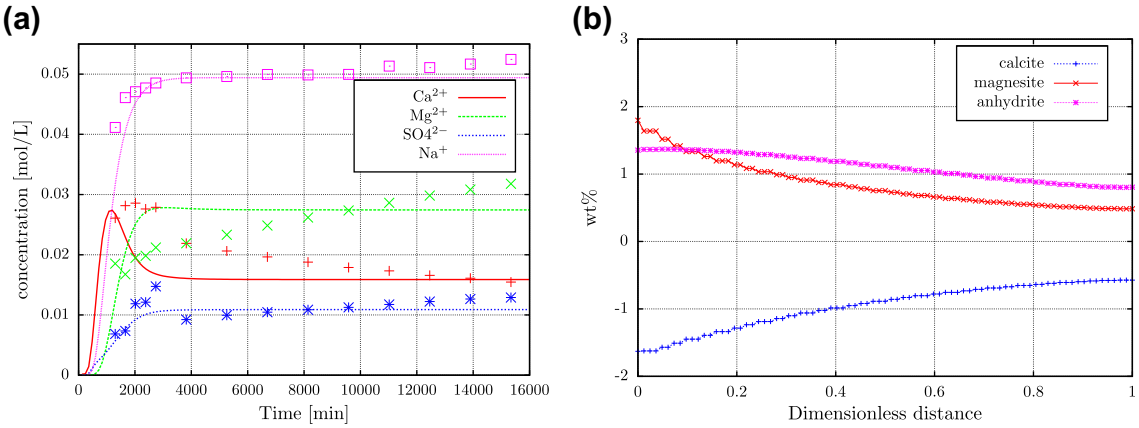

Fig. 3. (a) Effluent concentrations when seawater like brine ($Ca^{2+} = 0.013$, $Mg^{2+} = 0.0445$, $Cl = 0.1251$, $HCO_3^- = 0.002$, $K = 0.01$, $SO_4^{2-} = 0.024$, and $Na = 0.05$ mol/L) is flooded into a Liege chalk core at 130 °C. The solid curves are the LB predictions of the total concentration of the basis species indicated, and the data points the measured total concentrations. A CEC of 0.125 mol/L is used. (b) Mineralogical alteration along the plates (core) after 11 days of flooding.

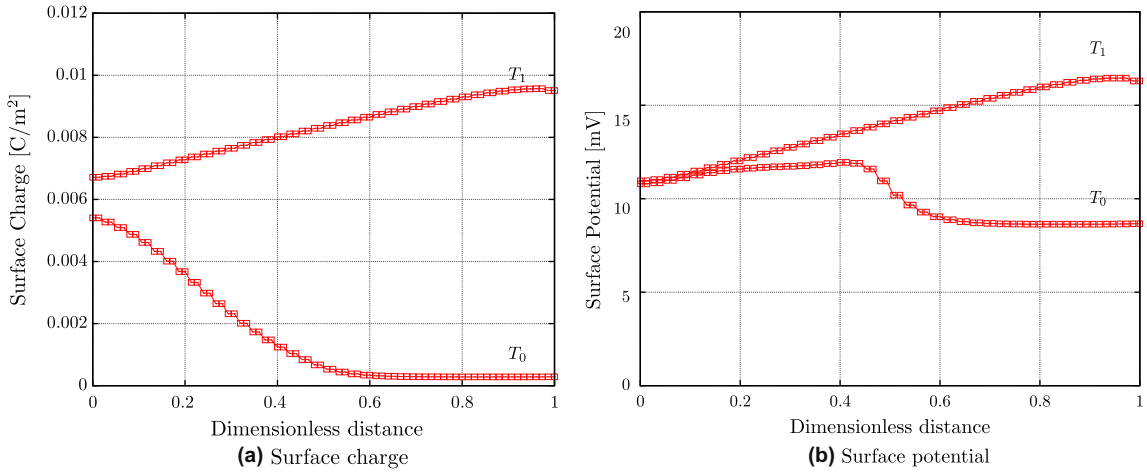

Fig. 4. The surface charge (a) and surface potential (b) along the flow direction at $T_0 = 120$ min, and at steady state, T_1, when seawater with a low concentration of NaCl is constantly injected at 1 PV/day. Distilled water is present initially.

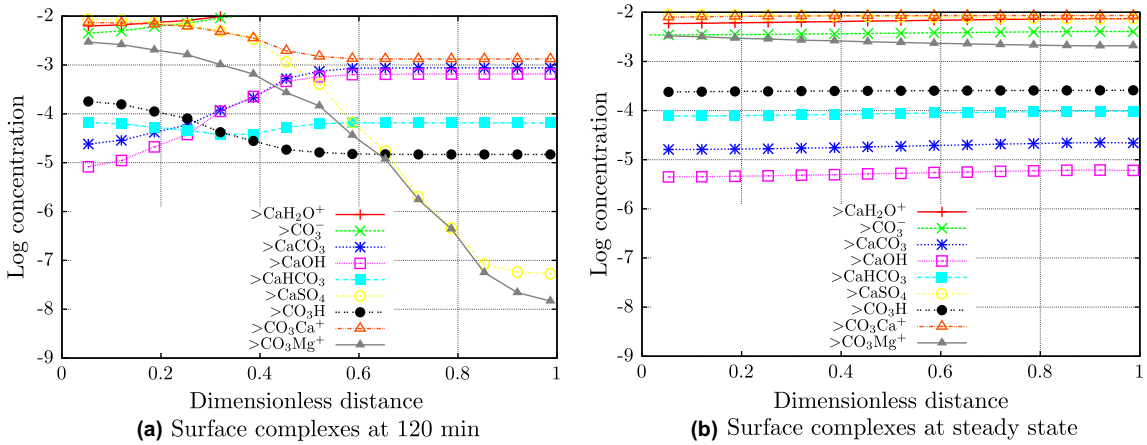

Fig. 5. The $\log_{10}$ concentration of surface complexes along the core.

kinetic parameters and anhydrite precipitation kinetics similar to those found in other experiments. The LB model does not capture the slow chemical trends that are observed in the later periods of the experiment. The slow trends could be caused by changes in the reactive surface area of calcite, as discussed in Arvidson et al. (2003), or by magnesite covering part of the exposed calcite surface. The trends could also be due to changes in surface roughness caused by dissolution of calcite. These imperfections are minor. What is remarkable to us is how well the model fits the core data with minimal or reasonable adjustments of kinetic data taken from completely independent determinations reported in the literature.

The LB model predicts the profiles of surface charge and surface potential that should exist along the laboratory cores. These predictions could be immediately used to evaluate hypotheses regarding how surface charge changes oil wettability and how surface potential might affect chalk strength. We do not relate the chemical changes we predict to observed changes in chalk strength or oil wettability (Evje and Hiorth, 2010; Hiorth et al., 2010; Madland et al., 2011). In this paper our main purpose is to describe a general chemical LB simulation method that includes nonlinear reaction kinetics and a general surface morphology, and show how it can be applied to core experiments. Application to compaction and oil recovery will be made in subsequent publications.

ACKNOWLEDGMENTS

The authors would like to thank the three anonymous reviewers for their valuable comments and suggestions to improve the manuscript, and the Research Council of Norway, BP Norge AS and the Valhall co-venturers, including Hess Norge AS, ConocoPhillips and the Ekofisk co-venturers, including Total E& P Norge AS, ENI Norge AS, Statoil Petroleum AS and Petoro AS for financial support.

APPENDIX A. DERIVATION OF THE INLET BOUNDARY CONDITION

The high flow rate in the inflow tube and the geometry of the inlet dictates in core experiments there is essentially no diffusion of chemicals back into the source reservoir. The geometry of the LB simulation does not automatically honor this condition, however. Here we describe the boundary conditions to include this effect.

The flooding fluid has species concentrations c_i^{inlet} before it enters the core. We specify that the flooding fluid enters through a tight sieve at $x = 0$ so that the backwards diffusion through the sieve is practically zero. Then the flux of basis species, $c_i^{\text{inlet}}\vec{u}$, advected by the flooding fluid into the core must matched the species flux on the core side of the sieve:

$$\vec{n}\cdot\vec{q}|_{x=0} = c_i^{\text{inlet}}\vec{n}\cdot\vec{u}(x=0,y). \tag{A.1}$$

Eq. (16) shows how to relate a flux boundary condition to the g_i distribution, and the inlet boundary becomes

$$g_{\bar{\alpha}}^i - \tilde{g}_{\alpha}^i = (\omega_\alpha + \omega_{\bar{\alpha}})\frac{\vec{e}_{\bar{\alpha}}\cdot\vec{u}\,c_i^{\text{inlet}}}{C_2}. \tag{A.2}$$

The continuum version of Eq. (A.1), assuming that $\vec{q} = c_i\vec{u} - D\nabla\cdot c_i$, becomes

$$\frac{\vec{n}\cdot\vec{u}}{D}\left(c_i|_{x=0} - c_i^{\text{inlet}}\right) = \vec{n}\cdot\nabla c_i|_{x=0}. \tag{A.3}$$

APPENDIX B. LB SURFACE TO VOLUME RATIO

The boundary condition given by Eqs. (16) and (17) can be related to a macroscopic rate equation by considering a small control volume where the reaction between the fluid and the pore wall is the rate limiting process. We calculate the total surface flux into the fluid from considering the contribution from each link that intersects the boundary. Since all collisions at fluid nodes conserve mass (the mole numbers) the change in the number of moles of the ith species is the sum of the left hand part of Eq. (16) for all links bisected by the pore surface. This can be seen clearly if we dimensionalize the equation, using δ_x for the grid spacing and δ_t for the time step. With the lattice speed $c_{LB} = \delta_x/\delta_t$.

$$\sum_{\text{walllinks}}(g_{\bar{\alpha}}^i - g_\alpha^i)\delta_x^d = N^i(t+\delta_t) - N^i(t), \tag{B.1}$$

where d is the number of spacial dimension, and N^i is mole number of species i in the control volume. For a pore volume V, $N^i(t+\delta_t) - N^i(t) = Vdc_i$. Multiplying the right hand side of Eq. (16) with the LB unit volume and summing over all wall links we get:

$$\sum_{\text{wall links}}(\omega_\alpha + \omega_{\bar{\alpha}})\frac{\vec{e}_{\bar{\alpha}}\cdot\mathbf{n}J_{\text{R}}^i}{C_2}\delta_x^d = \left(\sum_{\text{wall links}}(\omega_\alpha+\omega_{\bar{\alpha}})\frac{\vec{e}_{\bar{\alpha}}\cdot\mathbf{n}}{C_2}c_{LB}\delta_x^{d-1}\right)\left(J_{\text{R}}^i\delta_t\right) = A_{\text{tot}}J_{\text{R}}^i\delta_t, \tag{B.2}$$

where A_{tot} is the approximation to the total reactive area in the control volume. Let V denote the the size of the control volume:

$$V\frac{\mathrm{d}c_i}{\mathrm{d}t} = A_{\text{tot}}J_{\text{R}}^i. \tag{B.3}$$

In Eqs. (B.3) and (B.2) we have assumed that A_{tot} is a good approximation to the real (mineral surface) area. To verify that this assumption is valid we need to calculate the sum given in the first parenthesis in Eq. (B.2). This can be done by assuming that J_{R}^i is constant over the control volume, so it is only the direction of the surface elements and the number and direction of the links that contribute to the sum. A surface element of size δ_x^{d-1} and direction $\vec{n}$ will on average bisect $\vec{e}_{\bar{\alpha}}\cdot\vec{n}/c_{LB}$ links in the direction $\bar{\alpha}$, for lattices with cubic (or square in two dimensions) positioning of nodes (An explanation for this is given below). We note that both vector $\vec{e}_\alpha$ and $\vec{e}_{\bar{\alpha}}$ are aligned with this direction. But here we use the notation, consistent with the bounce back direction such that $\vec{e}_{\bar{\alpha}}\cdot\vec{n} > 0$. To simplify the calculations we consider all surface elements with the same surface normal. We can represent this with the distribution $A(\vec{n})\mathrm{d}n$, where dn represents an infinitesimal angle in $d = 2$ and a solid angle in $d = 3$, so that $A(\vec{n})\mathrm{dn}$ is the part of the surface area that have surface normals that do not differ by more than dn from $\vec{n}$. We can now approximate the sum over links in Eq. (B.2) by an integral over all normal directions and a sum over the contribution from each basis directions:

$$\sum_{\text{wall links}}(\cdots)\approx\oint\left(\sum_{\substack{\vec{\alpha}\\ \vec{e}_{\vec{\alpha}}\cdot\vec{n}>0}}\frac{\vec{e}_{\vec{\alpha}}\cdot\vec{n}}{c_{LB}}(\cdots)\right)\frac{A(\vec{n})}{\delta_x^{d-1}}\mathrm{d}n, \tag{B.4}$$

where the dots represents the summand in Eq. (B.2). Inserting the expression from Eq. (B.2) into the sum in the integrand on the right hand side in Eq. (B.4) we get:

$$\begin{aligned}\sum_{\substack{\vec{\alpha}\\ \vec{e}_{\vec{\alpha}}\cdot\vec{n}>0}}\frac{\vec{e}_{\vec{\alpha}}\cdot\vec{n}}{c_{LB}}(\cdots)&=\sum_{\substack{\vec{\alpha}\\ \vec{e}_{\vec{\alpha}}\cdot\vec{n}>0}}(\omega_\alpha+\omega_{\vec{\alpha}})\left(\frac{\vec{e}_{\vec{\alpha}}\cdot\mathbf{n}}{\sqrt{C_2}}\right)^2\delta_x^{d-1}\\&=\sum_{\substack{\vec{\alpha}\\ \vec{e}_{\vec{\alpha}}\cdot\vec{n}>0}}\omega_{\vec{\alpha}}\left(\frac{\vec{e}_{\vec{\alpha}}\cdot\mathbf{n}}{\sqrt{C_2}}\right)^2\delta_x^{d-1}\\&\quad+\sum_{\substack{\alpha\\ \vec{e}_\alpha\cdot\vec{n}<0}}\omega_\alpha\left(\frac{\vec{e}_\alpha\cdot\mathbf{n}}{\sqrt{C_2}}\right)^2\delta_x^{d-1},\end{aligned} \tag{B.5}$$

where we have split the sum into to parts by using the identities $\omega_\alpha=\omega_{\vec{\alpha}}$, and $\vec{e}_\alpha=-\vec{e}_{\vec{\alpha}}$. We note these two sums together is equivalent to one sum over all α's, hence:

$$\sum_\alpha\omega_\alpha\left(\frac{\vec{e}_\alpha\cdot\mathbf{n}}{\sqrt{C_2}}\right)^2\delta_x^{d-1}=C_2\frac{\vec{n}\cdot\vec{n}}{C_2}\delta_x^{d-1}=\delta_x^{d-1}. \tag{B.6}$$

Hence (B.4) can now be written:

$$\oint A(\vec{n})\mathrm{d}n\approx A_{\text{tot}}. \tag{B.7}$$

The crucial approximation is the average number of bisections. The calculated value is an ensemble average whereas it shows up as an self average in the integral over the surface. Increasing the resolution will increase the quality of this approximation.

We now discuss the relationship between the links that intersects the surface (wall) of a pore and the surface area of the pore. The basic idea is to calculate the density of bisection in a plane with the same direction as α, and use this to calculate the density of bisections for an arbitrary oriented surface. We make a solid by bisecting this plane with planes that have with normals along the coordinate axes, similar to Cauchy's tetrahedron construction in continuum mechanics. Fig. 6 shows this construction in two dimensions. If we consider a surface with an area, A, then the area A_i of each plane in the coordinate direction, i, is given by the projection of A:

$$A_i=A|e_{\alpha,i}|/|\vec{e}_\alpha|. \tag{B.8}$$

Since the nodes are position on a cubic lattice, the number nodes on each projected area is A_i/δ_x^{d-1}, where δ_x is the lattice spacing. Now if $|e_{\alpha,i}/c_{LB}|=1$ each node on A_i has a link that is bisected by A_i. The surface areas, A_i together with A makes a closed solid, each link that bisects one of the coordinate areas will also bisect A. Hence, the number of links bisected by A is the sum of the bisection of each A_i, which is equal to:

$$\sum_i\left(\frac{A_i}{\delta_x^{d-1}}\right)\frac{|e_{\alpha,i}|}{c_{LB}}=\sum_i A\frac{|e_{\alpha,i}|}{|\vec{e}_\alpha|\delta_x^{d-1}}\frac{|e_{\alpha,i}|}{c_{LB}}=A\frac{|\vec{e}_\alpha|}{\delta_x^{d-1}c_{LB}}. \tag{B.9}$$

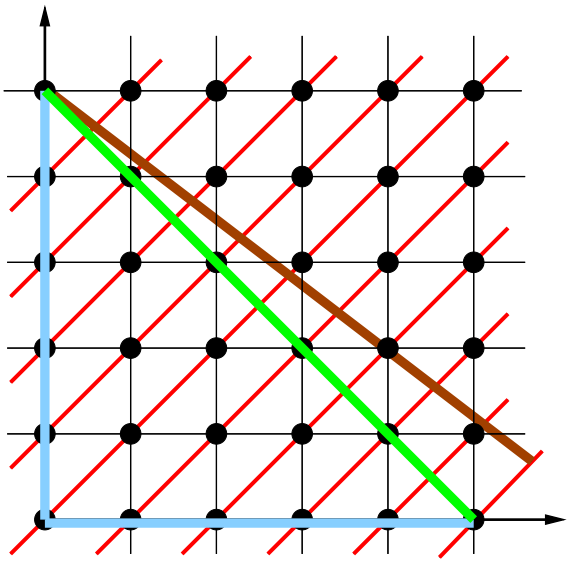

Fig. 6. An illustration of the construction to get the density of bisection. The links in the α direction are shown in red. The brown line indicates a plane with a surface normal $\vec{n}, A_n$. The green line shows the projection of A_n onto a plane with with a surface normal in the α direction. The blue lines indicates the projection of the green plane onto the coordinate axes. (For interpretation of the references to colour in this figure legend, the reader is referred to the web version of this article.)

This equation gives the density of bisection points for a surface with a normal in the α-direction. To get the density in a general direction, $\vec{n}$, we can project the surface element, with area A_n, onto the α-direction. The projected area has as many bisections as the original surface element, since it is projected along the direction of the links, and the result is the desired density:

$$\left(A_n\frac{\vec{e}_\alpha}{|\vec{e}_\alpha|}\cdot\vec{n}\right)\left(\frac{|\vec{e}_\alpha|}{\delta_x^{d-1}c_{LB}}\right)=\frac{\vec{e}_\alpha\cdot\vec{n}}{c_{LB}}\frac{A_n}{\delta_x^{d-1}}. \tag{B.10}$$

Similar arguments can also be used for the triangular case, except that we get a factor $2/\sqrt{3}$ in front of the expression above. This is canceled due the fact that the area assigned to a node on the triangular lattice is $(\sqrt{3}/2)\delta_x^2$.

REFERENCES

Appelo C. (1994) Cation and proton exchange, pH variations, and carbonate reactions in a freshening aquifer. *Water Resour. Res.* **30**(10), 2793–2805.

Arvidson R., Ertan I., Amonette J. and Luttge A. (2003) Variation in calcite dissolution rates: A fundamental problem? *Geochim. Cosmochim. Acta* **67**(9), 1623–1634.

Bethke C. M. (1996) Geochemical Reaction Modeling. Oxford University Press, New York.

Borkovec M. and Westall J. (1983) Solution of the Poisson–Boltzmann equation for surface excesses of ions in the diffuse layer at the oxide–electrolyte interface. *J. Electroanal. Chem.* **150**, 325–337.

Bouzidi M., Firdaouss M. and Lallemand P. (2001) Momentum transfer of a Boltzmann-lattice fluid with boundaries. *Phys. Fluids* **13**, 3452–3459.

Cali A., Succi S., Cancelliere A., Benzi R. and Gramignani M. (1992) Diffusion and hydrodynamic dispersion with the lattice Boltzmann method. *Phys. Rev. A* **45**(8), 5771–5774.

Cathles L. M. (2006) Eqalt-equilibrium chemical alteration. In *Combined Physical and Chemical Geofluids Modeling*. University of Windsor, Windsor, Ontario.

Chen S., Dawson S., Doolen G., Janecky D. and Lawniczak A. (1995) Lattice methods and their applications to reacting systems. *Comput. Chem. Eng.* **19**(6-7), 617–646.

Chen S. and Doolen G. D. (1998) Lattice Boltzmann method for fluid flows. *Annu. Rev. Fluid Mech.* **30**, 329–364.

Davis J. A. and Kent D. B. (1990) Surface complexation modeling in aqueous geochemistry. *Rev. Mineral.* **23**, 177–260.

Dawson S., Chen S. and Doolen G. (1993) Lattice Boltzmann computations for reaction–diffusion equations. *J. Chem. Phys.* **98**(2), 1514–1523.

Evje S. and Hiorth A. (2010) A mathematical model for dynamic wettability alteration controlled by water–rock chemistry. Networks and Heterogeneous Media 5.

Flukiger F. and Bernard D. (2009) A new numerical model for pore scale dissolution of calcite due to CO_2 saturated water flow in 3D realistic geometry: principles and first results. *Chem. Geol.* **265**(1-2), 171–180.

Gaines G. L. and Thomas H. C. (1953) Adsorption studies on clay minerals, ii, a formulation of the thermodynamics of exchange adsorption. *J. Chem. Phys.* **21**, 714–718.

He X., Zou Q., Luo L. and Dembo M. (1997) Analytic solutions of simple flows and analysis of nonslip boundary conditions for the lattice Boltzmann BGK model. *J. Stat. Phys.* **87**, 115–136.

Helgeson H. and Kirkham D. (1974a) Theoretical prediction of the thermodynamic behavior of aqueous electrolytes at high pressures and temperatures: I. Summary of the thermodynamic/electrostatic properties of the solvent. *Am. J. Sci.* **274**, 1089–1198.

Helgeson H. and Kirkham D. (1974b) Theoretical prediction of the thermodynamic behavior of aqueous electrolytes at high pressures and temperatures: II. Debye-huckel parameters for activity coefficients and relative partial molal properties. *Am. J. Sci.* **274**, 1089–1198.

Helgeson H., Kirkham D. and Flowers G. (1981) Theoretical prediction of the thermodynamic behavior of aqueous electrolytes by high pressures and temperatures: IV. Calculation of activity coefficients, osmotic coefficients, and apparent molal and standard and relative partial molal properties to 600 °C and 5 kb. *Am. J. Sci.* **281**, 1249–1516.

Hiorth A., Cathles L. M. and Madland M. V. (2010) The impact of pore water chemistry on carbonate surface charge and oil wettability. *Trans. Porous Media*, 85.

Israelachivili J. (1985) Intermolecular and Surface Forces. Academic Press, New York City.

Jerauld G., Lin C., Webb K. and Seccombe J. (2006) Modeling low-salinity waterflooding. In: *The 2006 SPE Annual Technical Conf. & Exhib.*, San Antonio, Texas, USA, 24–27 September, SPE102239.

Johnson J. W., Oelkers E. H. and Helgeson H. (1992) Supcrt92: A software package for calculating the standard molal thermodynamic properties of minerals, gases, aqueous species, and reactions from 1 to 5000 bar and 0 to 1000 °C. *Comp. Geol. Sci.* **18**(7), 899–947.

Kang Q. J., Lichtner P. C. and Janecky D. R. (2010a) Lattice boltzmann method for reacting flows in porous media. *Adv. Appl. Math. Mech.* **2**(5), 545–563.

Kang Q. J., Lichtner P. C., Viswanathan H. S. and Abdel-Fattah A. I. (2010b) Pore scale modeling of reactive transport involved in geologic CO_2 sequestration. *Trans. Porous Media* **82**(1), 197–213.

Kang Q. J., Lichtner P. C. and Zhang D. (2007) An an improved lattice Boltzmann model for multicomponent reactive transport in porous media at the pore scale. *Water Resour. Res.*, 43.

Kingdon R. and Schofield P. (1992) A reaction-flow lattice Boltzmann model. *J. Phys. A: Math. General* **25**(14), L907–L910.

Lallemand P. and Luo L. (2003) Lattice Boltzmann method for moving boundaries. *J. Comp. Phys.* **184**, 406–421.

Lasaga A. C. (1998). *Kinetic theory in the earth sciences*. .

Li L., Steefel C. I. and Yang L. (2008) Scale dependence of mineral dissolution rates within single pores and fractures. *Geochim. Cosmochim. Acta* **72**(2), 360–377.

Madland M. V., Hiorth A., Korsnes R. I., Evje S. and Cathles L. (2009) Rock fluid interactions in chalk exposed to injection of seawater, $MgCl_2$, and $NaCl_2$ brines with equal ionic strength. *EAGE-2009*, A22.

Madland M. V., Hiorth A., Omdal E., Megawati M., Hildebrand-Habel T., Korsnes R. I., Evje S. and Cathles L. M. (2011) Chemical alterations induced by rock–fluid interactions when injecting brines in high porosity chalks. *Trans. Porous Media* **87**(3), 679–702.

Molins S., Trebotich D., Steefel C. I. and Shen C. (2012) An investigation of the effect of pore scale flow on average geochemical reaction rates using direct numerical simulation. *Water Resour. Res.*, 48.

Morse J. W. and Berner R. A. (1972) Dissolution kinetics of calcium carbonate in seawater: II. A kinetic origin for lysocline. *Am. J. Sci.* **272**, 840–851.

Oelkers E. H., Benezeth P. and Pokrovski G. S. (2009) Thermodynamic databases for water–rock interaction. *Thermodyn. Kinet. Water–Rock Interact.* **70**, 1–46.

Palandri J. L. and Kharaka K. Y. (2004) A compilation of rate parameters of water–mineral interaction kinetics for application to geochemical modeling. Tech. rep., U.S. Geological Survey.

Parkhurst D. L. and Appelo C. A. J. (1999) User's guide to phreeqc (version 2) – a computer program for speciation, batch-reaction, one-dimensional transport, and inverse geochemical calculations. U.S. Geol. Survey, Water-Resour. Inv. Rep. 99-4259. <www.xs4all.nl/ appt>.

Plummer L. N., Wigley T. M. L. and Parkhurst D. L. (1978) The kinetics of calcite dissolution in CO_2–water systems at 5 to 60 °C and 0.0 to 1.0 atm CO_2. *Am. J. Sci.* **278**, 179–216.

Pokrovsky O. and Schott J. (1999) Processes at the magnesium-bearing carbonates/solution interface: II. Kinetics and mechanism of magnesite dissolution. *Geochim. Cosmochim. Acta* **63**(6), 881–897.

Pokrovsky O. and Schott J. (2001) Kinetics and mechanism of dolomite dissolution in neutral to alkaline soloutions revisited. *Am. J. Sci.* **301**, 597–626.

Pokrovsky O. and Schott J. (2002) Surface chemistry and dissolution kinetics of divalent metal carbonates. *Environ. Sci. Technol.* **36**, 426–432.

Pokrovsky O., Schott J. and Thomas F. (1999a) Dolomite surface speciation and reactivity in aquatic systems. *Geochim. Cosmochim. Acta* **63**(19/20), 3133–3143.

Pokrovsky O., Schott J. and Thomas F. (1999b) Processes at the magnesium-bearing carbonates/solution interface: I. A surface speciation model for magnesite. *Geochim. Cosmochim. Acta* **63**(6), 863–880.

Saldi G. M., Jordan G., Schott J. and Oelkers E. H. (2009) Magnesite growth rates as a function of temperature and saturation state. *Geochim. Cosmochim. Acta* **73**, 5646–5657.

Steefel C. I. and MacQuarrie (1996) Approaches to modelling of reactive transport in porous media. In *Reactive Transport in Porous Media*, vol. 34 (eds. P. C. Lichtner, C. I. Steefel and E. H. Oelkers). Mineralogical Society of America.

Steefel C. J. and Van Cappelen P. (1990) A new kinetic approach to modeling water–rock interaction: the role of nucleation, precursors, and ostwald ripening. *Geochim. Cosmochim. Acta* **54**, 2657–2677.

Succi S. (2001) *The Lattice Boltzmann Equation, for Fluid Dynamics and Beyond*. Oxford University Press.

Sukop M. C. and Thorne D. T. (2006) *Lattice Boltzmann Modelling: An Introduction for Geoscientists and Engineers*. Springer.

Tang G. and Morrow N. R. (1999) Oil recovery by waterflooding and imbibition – invading brine cation valency and salinity. *SCA*, 11.

Van Cappelen P., Charlet L., Stumm W. and Wersin P. (1993) A surface complexation model of the carbonate mineral–aqueous solution interface. *Geochim. Cosmochim. Acta* **57**, 3505–3518.

Verhaeghe F., Arnout S., Blanpain B. and Wollants P. (2006) Lattice-Boltzmann modeling of dissolution phenomena. *Phys. Rev. E* **73**, 1–10.

Wagner R., Kühn M., Meyn V., Pape H., Vath U. and Clauser C. (2005) Numerical simulation of pore space clogging in geothermal reservoirs by precipitation of anhydrite. *Int. J. Rock Mech. Mining Sci.* **42**, 1070–1081.

Wolf-Gladrow D. (1995) A lattice Boltzmann-equation for diffusion. *J. Stat. Phys.* **79**(5–6), 1023–1032.

Yildiz H. O. and Morrow N. R. (1996) Effect of brine composition on recovery of moutray crude oil by waterflooding. *J. Pet. Sci. Eng.* **14**, 159–168.

Yoon H., Valocchi A. J., Werth C. J. and Dewers T. (2012) Pore-scale simulation of mixing-induced calcium carbonate precipitation and dissolution in a microfluidic pore network. *Water Resour. Res.*, 48.

Zhang P. M., Tweheyo M. T. and Austad T. (2007) Wettability alteration and improved oil recovery by spontaneous imbibition of seawater into chalk: impact of the potential determining ions Ca^{2+}, Mg^{2+}, and SO_4^{2-}. *Colloid. Surf. A: Physicochem. Eng. Aspects* **301**(1-3), 199–208.

Ziegler D. (1993) Boundary conditions for lattice Boltzmann simulations. *J. Stat. Phys.* **71**, 1171–1177.

Associate editor: Jacques Schott